New Magnetic Field Analysis Considering a Vector Magnetic Characteristic

Hiroyasu Shimoji*, Masato Enokizono*, Takashi Todaka* and Toyomi Horibe*

Abstract - This paper presents magnetic field analysis technology that uses a vector magnetic characteristic. Recently the magnetic material was found to be measurable using the vector quantity technique. Therefore considering the anisotropy of the magnetic material in the vector field analysis is necessary. The magnetic field analysis method, which is considered the anisotropy by combining the finite element method with the E&S^2 (Enokizono, Soda, and Shimoji) modeling, is applied to a permanent magnet motor model.

Keywords: material modeling, finite element method, and vector magnetic property

1. Introduction

Recently a measuring technique for two-dimensional magnetic characteristics has been developed and its achievements have drawn much attention [1]. The two-dimensional magnetic characteristics are the relationships between the measured magnetic flux density **B** and the magnetic field strength **H** as a vector quantity. Those data can express the magnetic anisotropy and iron loss precisely. We enable analysis of the magnetic anisotropy and nonlinearity that has been considered difficult [2-5]. Thus the tendency that iron loss increases when the phase difference between **B** and **H** occurs is well expressed in this method. The conventional analysis was unable to consider the phase difference between **B** and **H**. Therefore, considering complex characteristics in the magnetic materials was difficult. Use of the complex characteristics in the magnetic field analysis is important in designing high efficiency electrical machinery; complex characteristics of the magnetic materials must be considered for the magnetic field analysis. We have analyzed a three-phase induction motor model and the permanent magnet motor by using the improved finite element method considering the vector magnetic properties. This method is very useful in designing low loss and high efficient motors. In this paper, we discuss and present the effect of some core constructions that has low loss, by using this method.

1.1 Two-dimensional magnetic measuring apparatus

Fig.1 shows the outline of the two-dimensional magnetic measuring apparatus and measurement system.

The yoke for the excitation is placed for the two-directional excitation in X-axis direction and Y-axis direction. In addi-

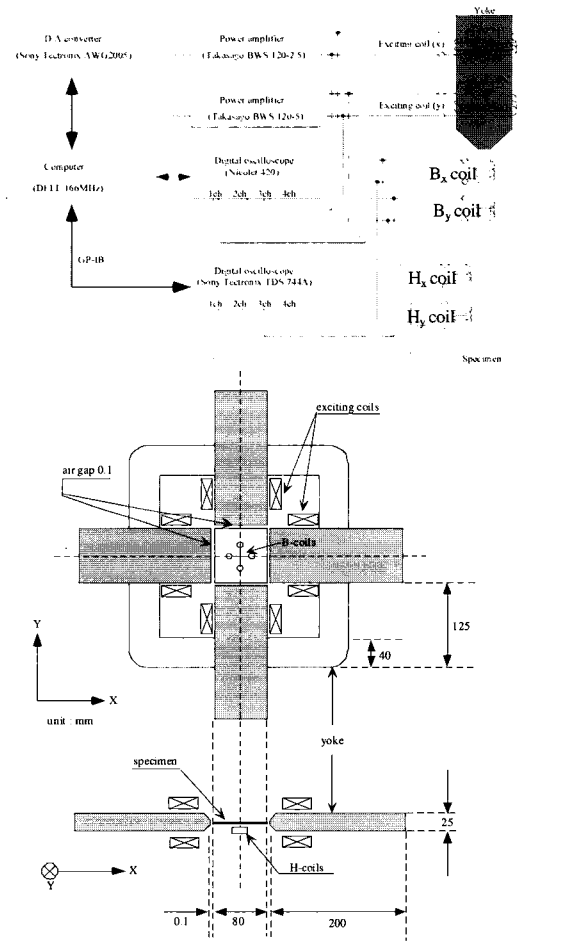

Fig. 1 Two-dimensional magnetic measuring apparatus and measurement system.

* Dept. of Electrical and Electronic Engineering, Oita University Japan (simoji@cc.oita-u.ac.jp, enokizono@cc.oita-u.ac.jp)
Received February 27, 2002 ; Accepted September 15, 2002

tion, the air gap is made by putting 0.1mm sheets between the sample and the excitation yoke because of equalizing a magnetic flux inside of the sample. The rotational magnetic flux in any direction can be generated by the two-directional excitation.

1.2 The anisotropy of the magnetic material

Fig. 2 shows an alternating magnetic flux and a rotating magnetic flux. The alternating magnetic flux can be defined by the maximum magnetic flux density and the inclination angle Φ from the easy axis. The rotating magnetic flux can be defined by the axis ratio Φ and the maximum magnetic flux density and the inclination angle Φ from the easy axis. The easy axis direction and the hard axis direction exist in any magnetic material. For example, Fig. 3 shows the magnetic field loop of a non-oriented silicon steel sheet, which has the hard axis direction near 45 degrees through 120 degrees. Fig. 4 shows the magnetic field loop of the grain-oriented silicon steel sheet having the hard axis direction near 90 degrees. Fig. 5 shows the magnetic field loop of the double grain-oriented silicon steel sheet having the hard axis direction near 45 degrees and 130 degrees. In these measurements, the flux density trajectory was controlled to be a real circle.

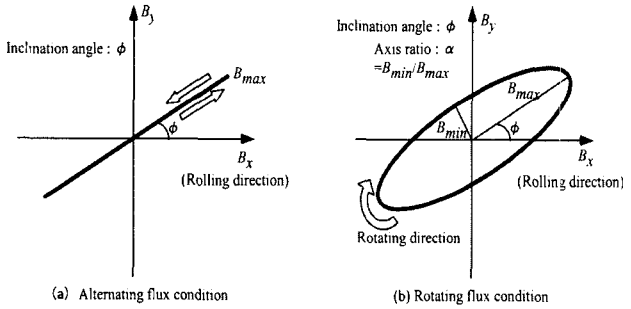

Fig. 2 Representation of alternating and rotating flux

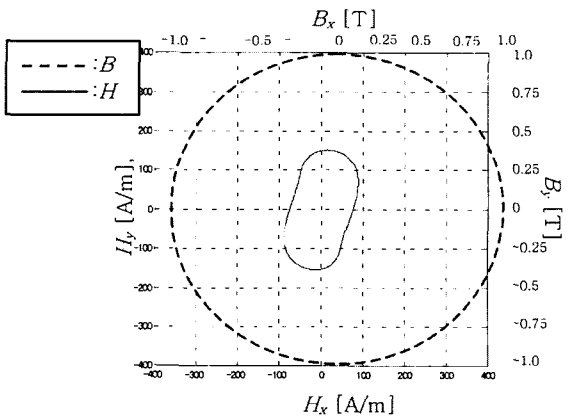

Fig. 3 The magnetic field measured in rotation flux condition (sample: non-oriented silicon steel sheet, α =1, B_{max}=1 [T]).

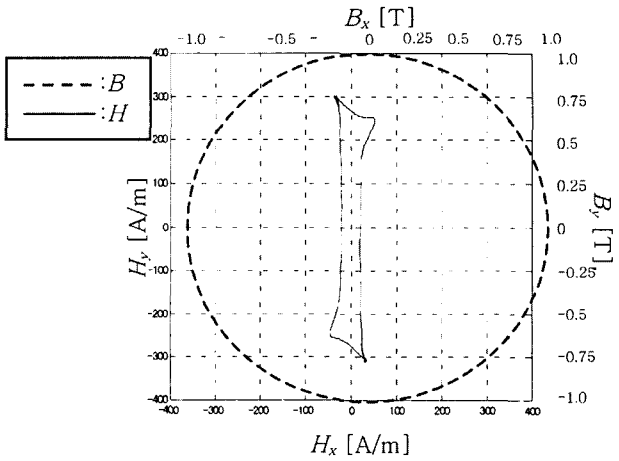

Fig. 4 The magnetic field measured in rotation flux condition(sample: grain-oriented silicon steel sheet, α =1, B_{max}=1 [T]).

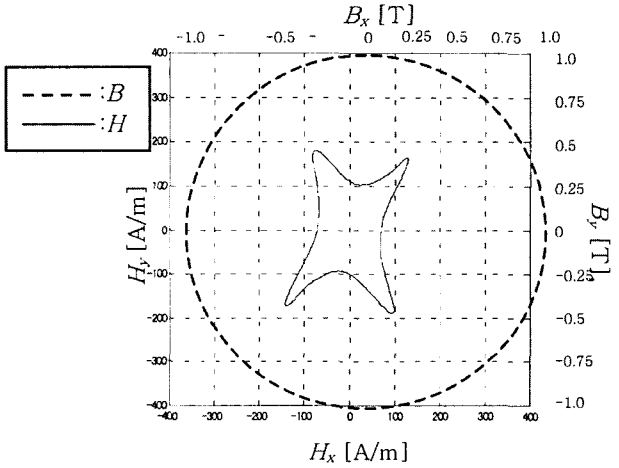

Fig. 5 The magnetic field measured in rotation flux condition(sample: double grain-oriented silicon steel sheet, α =1, B_{max}=1 [T]).

2. The Finite Element Method with the E&S^2 Modeling

2.1 The E&S^2 modeling

The E&S^2 modeling is defined with the following equation [3].

$$\begin{cases} H_x = \upsilon_{xr} B_x + \upsilon_{xi} \int B_x d\theta \\ H_y = \upsilon_{yr} B_y + \upsilon_{yi} \int B_y d\theta \end{cases} \quad (1)$$

where v_{xr}, v_{xi}, v_{yr} *and* v_{xr} are the reluctivity coefficients. v_{xr}, v_{xi}, v_{yr} *and* v_{xr} are expressed as follows.

$$\begin{cases} \upsilon_{xr} = k_{xr1} + k_{xr2}B_x + k_{xr3}B_x\left(\dfrac{\partial B_x}{\partial t}\right) + k_{xr4}\left(\dfrac{\partial B_x}{\partial t}\right)^2 \\ \upsilon_{xi} = k_{xi1} + k_{xi2}B_x + k_{xi3}B_x\left(\dfrac{\partial B_x}{\partial t}\right) + k_{xi4}\left(\dfrac{\partial B_x}{\partial t}\right)^2 \\ \upsilon_{yr} = k_{yr1} + k_{yr2}B_y + k_{yr3}B_y\left(\dfrac{\partial B_y}{\partial t}\right) + k_{yr4}\left(\dfrac{\partial B_y}{\partial t}\right)^2 \\ \upsilon_{yi} = k_{yi1} + k_{yi2}B_y + k_{yi3}B_y\left(\dfrac{\partial B_y}{\partial t}\right) + k_{yi4}\left(\dfrac{\partial B_y}{\partial t}\right)^2 \end{cases} \quad (2)$$

The coefficients k_{xrn}, k_{xin}, k_{yrn}, and k_{yin} (n 1,2,3,4) are obtained from the measurement data. The magnetic flux density and the magnetic field intensity are approximated with the following equations expressed by the Fourier expansion.

$$\begin{cases} B_x = A_{B_x 1}\cos\omega t - B_{B_x 1}\sin\omega t \\ B_y = A_{B_y 1}\cos\omega t - B_{B_y 1}\sin\omega t \end{cases} \quad (3)$$

$$\begin{cases} H_x = \sum_{1}^{2} A_{H_x(2n-1)}\cos\omega t - B_{H_x(2n-1)}\sin\omega t \\ H_y = \sum_{1}^{2} A_{H_y(2n-1)}\cos\omega t - B_{H_y(2n-1)}\sin\omega t \end{cases} \quad (4)$$

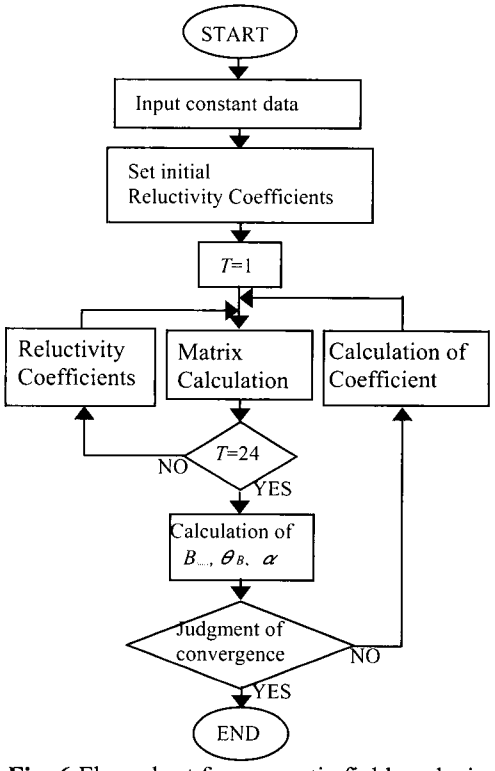

Fig. 6 Flow chart for magnetic field analysis.

Fig. 6 shows the flow-chart of this analysis. Because the components of the reluctivity coefficients have non-linearly, calculating iteratively is necessary. We can carry out the non-liner magnetic field analysis considering both alternating and rotating hysteresis with this modeling. Then, we can obtain directly the distribution of iron loss in the core.

Fig. 7 shows the measurement data with the Two-dimensional magnetic measuring apparatus. The inclination angle was 30 degrees, and the axis ration was 0.2. Fig. 8 shows the calculated field intensity H by using E&S^2 modeling. We can see that this modeling is a fairly good approximation.

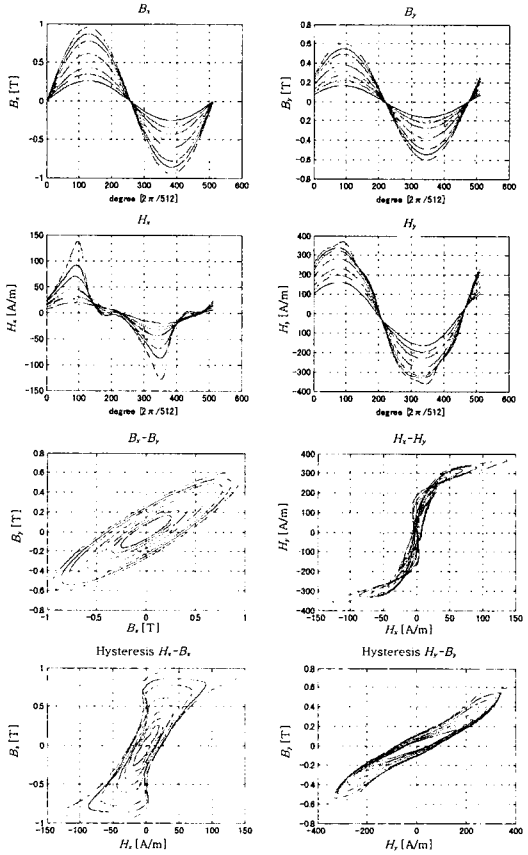

Fig. 7 Measurements data from two-dimensional magnetic measuring apparatus (B_{max}=0.5～1.1, α=0.21, Inclination=31 degree).

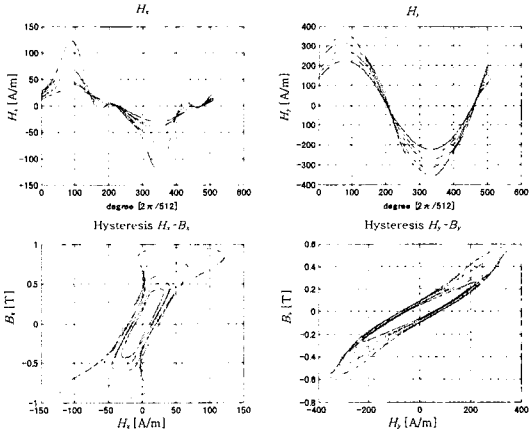

Fig. 8 The calculation data by using E&S^2 modeling (B_{max}=0.5～1.1, α=0.2,1 Inclination=31 degree).

2.2 Formulation of magnetic field analysis

Substituting (1) into the Maxwell's equation in the two-dimensional transient magnetic field, we can obtain the following equation.

$$J_0 + J_m = \frac{\partial}{\partial x}\left(a_3 \frac{\partial A_z}{\partial y} - a_4 \frac{\partial A_z}{\partial x} \right) - \frac{\partial}{\partial y}\left(a_1 \frac{\partial A_z}{\partial y} - a_2 \frac{\partial A_z}{\partial x} \right) + \frac{\partial}{\partial \theta}\left\{ \frac{\partial}{\partial x}\left(b_3 \frac{\partial A_z}{\partial y} - b_4 \frac{\partial A_z}{\partial x} \right) - \frac{\partial}{\partial y}\left(b_1 \frac{\partial A_z}{\partial y} - b_2 \frac{\partial A_z}{\partial x} \right) \right\} \quad (5)$$

$$\begin{cases} a_1 = \cos^2(\phi)\nu_{xr} + \sin^2(\phi)\nu_{yr} \\ a_2 = a_3 = \sin(\phi)\cos(\phi)\nu_{xr} - \sin(\phi)\cos(\phi)\nu_{yr} \\ a_4 = \sin^2(\phi)\nu_{xr} + \cos^2(\phi)\nu_{yr} \end{cases} \quad (6)$$

$$\begin{cases} b_1 = \cos^2(\phi)\nu_{xi} + \sin^2(\phi)\nu_{yi} \\ b_2 = b_3 = \sin(\phi)\cos(\phi)\nu_{xi} - \sin(\phi)\cos(\phi)\nu_{yi} \\ b_4 = \sin^2(\phi)\nu_{xi} + \cos^2(\phi)\nu_{yi} \end{cases} \quad (7)$$

where J_0 is the exciting current density, J_m is the magnetization, A ($=A_z$) is the magnetic vector potential, and ϕ is the inclination angle of and the easy axis from the X-axis.

Because the components of reluctivity coefficients, $\nu_{xr}, \nu_{xi}, \nu_{yr}, and\ \nu_{xr}$, have non-linearity, those values must be calculated iteratively until they. We can carry out the non-linear magnetic field analysis considering the hysteresis.

The two-dimensional governing equation of the induction motor considering the E&S^2 model is written as follows.

$$\frac{\partial}{\partial x}\left(\nu_{rxy} \frac{\partial A}{\partial x} \right) - \frac{\partial}{\partial x}\left(\nu_{rxx} \frac{\partial A}{\partial y} \right) - \frac{\partial}{\partial y}\left(\nu_{ryy} \frac{\partial A}{\partial x} \right) + \frac{\partial}{\partial y}\left(\nu_{ryx} \frac{\partial A}{\partial y} \right) + \frac{\partial}{\partial \theta}\left\{ \frac{\partial}{\partial x}\left(\nu_{ixy} \frac{\partial A}{\partial x} \right) - \frac{\partial}{\partial x}\left(\nu_{ixx} \frac{\partial A}{\partial y} \right) - \frac{\partial}{\partial y}\left(\nu_{iyy} \frac{\partial A}{\partial x} \right) + \frac{\partial}{\partial y}\left(\nu_{iyx} \frac{\partial A}{\partial y} \right) \right\} = -J_0 + \sigma\left\{ \frac{\partial A}{\partial t} + \frac{\partial \varphi}{\partial z} - \omega_s(1-s)\left(y\frac{\partial A}{\partial x} - x\frac{\partial A}{\partial y} \right) \right\} \quad (8)$$

where φ is the electric scalar potential, σ is the conductivity, ω_s the synchronous angular velocity, and s is the slip.

On the other hand, the circuit equation is written as

$$V_{0n} = \frac{\partial}{\partial t}\int_c A ds + R_{mn} I_{nm} \quad (9)$$

where $V_{0n}\ (n = 1 \sim 3)$ is the terminal voltage, R_{mn} the resistance of an exciting coil, and I_{mn} the exciting current. $\partial\varphi/\partial z$ can be derived with the charge conservation law.

$$\frac{\partial \varphi}{\partial z} = -\frac{1}{S_t}\iint_{S_t}\left\{ \frac{\partial A}{\partial t} - \omega_s(1-s)\left(y\frac{\partial A}{\partial x} - x\frac{\partial A}{\partial y} \right) \right\} dS \quad (10)$$

Combining (8), (9) and (10), the exciting current I_m can be treated as an unknown value. Furthermore, we can obtain both of the **H**-vector and the **B**-vector distributions.

2.3 Iron Loss

The iron loss and total iron loss can be calculated directly from the analyzed results by using the following equations:

$$P_i = \frac{1}{\rho T}\int_0^T \left(H_x \frac{dB_x}{dt} + H_y \frac{dB_y}{dt} \right) dt \quad [\mathrm{W/kg}] \quad (11)$$

$$Pt_{total} = \rho \cdot D_p \cdot N_{os} \cdot \sum_{i=1}^{N_{es}} Pt_i \cdot S_i \quad [\mathrm{W}] \quad (12)$$

where D_p is the thickness of the electrical steel sheet, N_{os} the number of lamination of the sheet, N_{es} the number of finite elements in the core, P_{ti} the iron loss of a finite element (i),and S_i the area of a finite element. As a core material, the silicon steel sheet H30 class (produced by Nippon Steel Corporation) is assumed. D_p was 0.5 [mm], ρ was 7850 [kg/m3], and N_{os} was 600.

3. Results and Discussions

Fig. 9 shows a permanent magnet motor model. The stator core is constructed of non-oriented silicon steel sheet. The permanent magnet has been placed in the rotor surface. Table 1 shows the easy axis direction of each tooth and the detailed analysis condition. Fig. 10 shows the obtained iron loss distributions. Total loss of model 1 was 0.43537 W and of model 2 was 0.42659 W. It is known that the total iron loss can be reduced by changing the easy axis direction. Therefore the total iron loss cannot be judged in quantity since it also increases when magnetic flux density increases. Fig. 10 also shows the distribution of the iron loss divided by the square of magnetic flux density. Model 2 is proven to be improved further than model 1.

Fig. 11 shows the various constricted stator core models. The direction of the arrow in the figures is the rolling direction, which is the easy axis of magnetizing. Fig. 13 shows the locus distribution of the **B**-vector and **H**-vector of the Type-1 and Type-3. Fig. 12 shows the distribution

of iron loss and Fig. 14 shows the speed characteristic of iron loss. From these figures, Type-1 has the lowest loss in the models. The main loss seems to be located in the stator yoke part.

Table 1

	Model 1 (degree)	Model 2 (degree)
Tooth 1	0 (x direction)	28
Tooth 2	0	119
Tooth 3	0	89
Tooth 4	0	59
Tooth 5	0	88
Tooth 6	0	58
Tooth 7	0	28
Tooth 8	0	118
Tooth 9	0	89
Tooth 10	0	120
Tooth 11	0	88
Tooth 12	0	118
Element number	34314	34314
Node number	17242	17242
The average of B_{max}	0.5800	0.5764

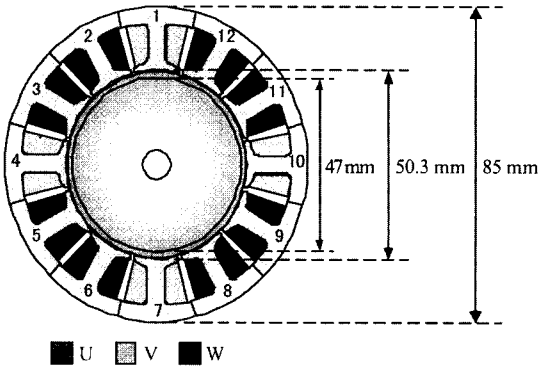

Fig. 9 Analysis model of the permanent magnet motor.

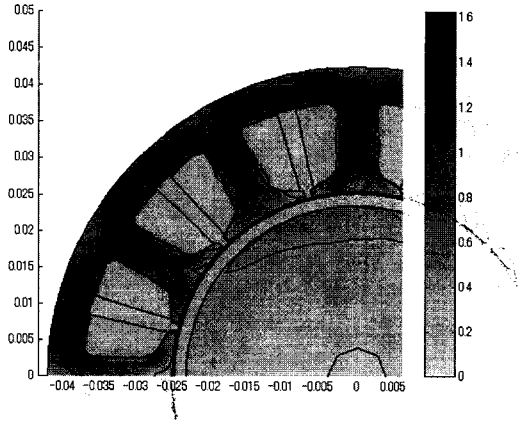

(Model 1)

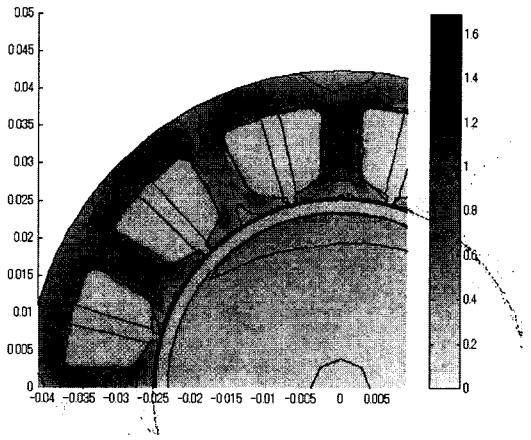

(Model 2)

Fig. 10 The core loss distribution [W/kg].

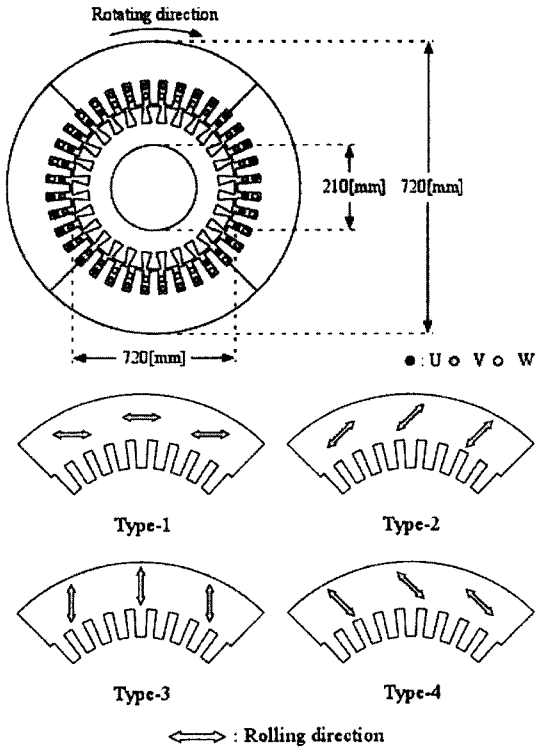

Fig. 11 Analytical model of induction motor core.

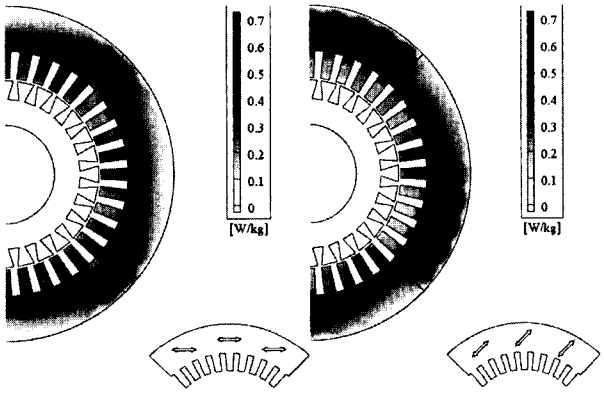

(a) Type-1 (b) Type-2

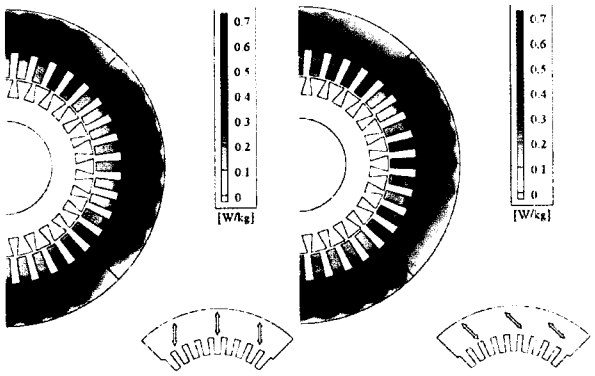

(a) Type-3 (b) Type-4

Fig. 12 Iron loss distribution.

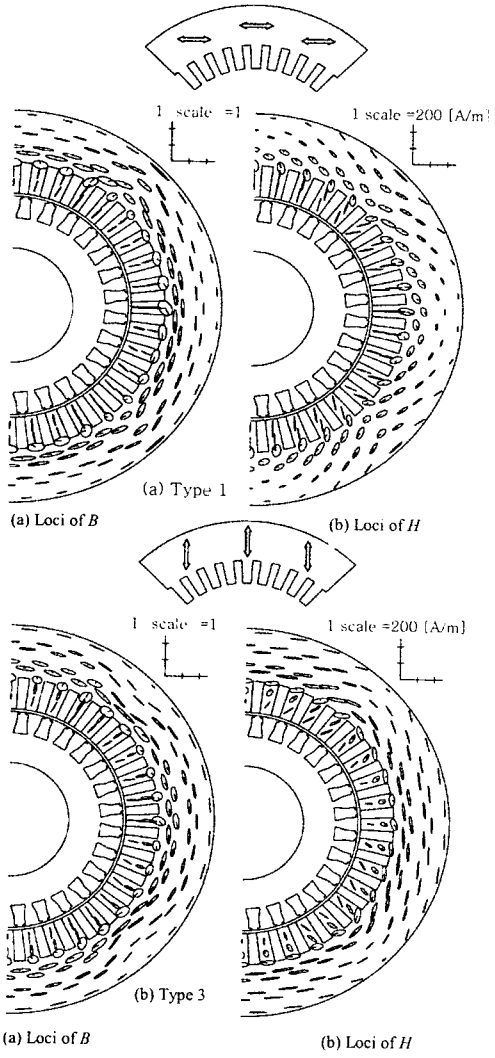

Fig. 13 Distribution of loci of **H** and **B**-vector.

Figs. 15 and 16 compare the maximum efficiency and the maximum loading torque. From the results, the construction of Type-1 also has the highest torque in these investigated models.

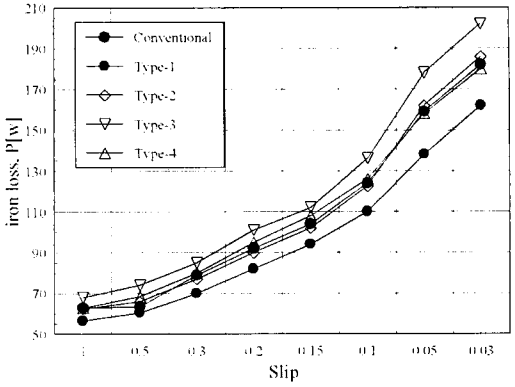

Fig. 14 Relationship between total iron loss and slip.

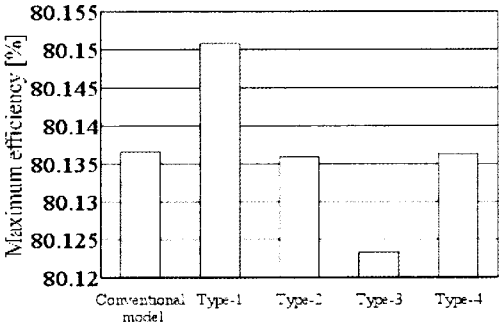

Fig. 15 Comparison of maximum efficiency.

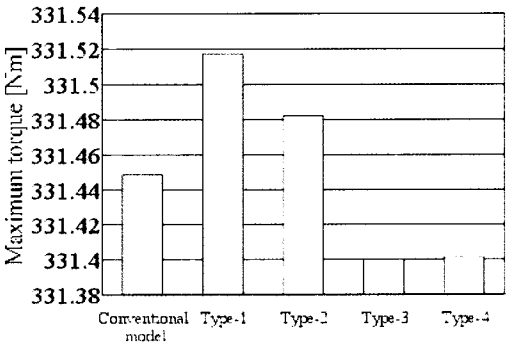

Fig. 16 Comparison of maximum torque.

4. Conclusions

The results are summarized as follows.

(1) The iron loss was analyzed directly by the improved analysis methods taking into account the vector magnetic hysteresis.

(2) The distribution of iron loss and the behavior of the **H**-vector and **B**-vector can be obtained to evaluate the motor models.

(3) The usefulness of this method, E&S^2 model, is practically assessed.

We have proposed the concept of measurable data: practical machines should be analyzed using this measurable data and its modeling.

References

[1] Sorin Aurel Spornic, Afef Kedous-Lebouc, and Bruno Cornut, "Anisotropy and Texture Influence on 2D Magnetic Behaviour for Silicon, Cobalt, and Nickel Iron Alloys," *Journal of Magnetism and Magnetic Materials,* Vols. 215-216, pp. 614-616, 2000.

[2] M. Enokizono, T. Todaka, S. Kanao, and J. Sievert, "Two-Dimensional Magnetic Properties of Silicon Sheet Subjected to a Rotating Field," *IEEE Trans. on Magnetics*, Vol. 29, No. 6, pp. 3550-3552, 1993.

[3] N. Soda and M. Enokizono, "E&S Hysteresis Model for Two-Dimensional Magnetic Properties," *Journal of Magnetism and Magnetic Materials,* Vols. 215-216, pp. 626-628, 2000.

[4] M. Enokizono and N. Soda, "Direct Magnetic Loss Analysis by FEM Considering Vector Magnetic Properties," *IEEE Trans. on Magnetics*, Vol. 34, No. 5, pp. 188-195, 1998.

[5] M. Enokizono, ed., "Two-Dimensional Magnetic Measurement and its Properties," Proceedings of the Second International Workshop on 2DMAG., JSAEM Studies in Applied Electromagnetic, Vol. 1 (1992).

[6] M. Enokizono and N. Soda, "Iron Loss Analysis of Three-Phase Transformer by using Finite Element Method," *Proc. ICEE* ' 8, Vol. 1, pp. 852-855, 1998.

[7] Y. Daito, S. Hayano, and H. Nakamula, "A Representation of Magnetic Hysteresis by Fourier Series," *Journal of Magnetism and Magnetic Materials,* Vol. 54-57, pp. 1613-1614, 1986.

Hiroyasu Shimoji

He graduated from Faculty of Engineering, Oita University in March 1998 with the degree of Bachelor. He is currently a ph. D course student at Oita University, JAPAN.

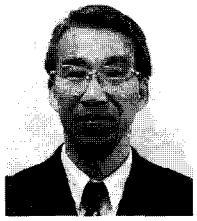

Masato Enokizono

He graduated from Kyushu Institute of Technology in March 1973 with the degree of Bachelor of Electrical Engineering., entered Postgraduate Course of Kyushu University, April 1973, obtained an M.S. degree in Electrical Engineering (Literal translation is Master of Engineering) in March 1975 and received a Dr. E. degree (Literal translation is Doctor of Engineering) in January 1979 from Kyushu University for a thesis entitled: "Studies on the High Silicon-Steel Sheet". He was a researcher of Kyushu University from February 1979 to January 1980. He got Research scholarship of Alexander von Humboldt-Stiftung in Phusikalisch-Technischen Bundesanstalt (PTB) Braunschweig, Lab. Magnetic Measurement Technique December 1986 to November 1987. He is currently a Professor at Department of Electric and Electronic Engineering, Faculty of Engineering, Oita University, JAPAN.

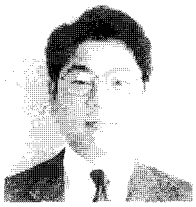

Takashi Todaka

He is currently a Professor at Department of Electric and Electronic Engineering Faculty of Engineering, Oita University, JAPAN

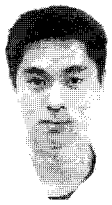

Toyomi Horibe

He graduated from Faculty of Engineering, Oita University in March 2001 with the degree of Bachelor. He is currently a master course student at Oita University, JAPAN.